Monatshefte für Chemie 135, 357–370 (2004)
DOI 10.1007/s00706-003-0081-6

Monatshefte für Chemie
Chemical Monthly
Printed in Austria

Structural and Catalytic Activity of V_2O_5-Supported on $AlPO_4$ Catalysts

Mohamed M. M. Abd El-Wahab[1], **Abd El-Aziz A. Said**[1,*], and **Shar S. Al-Shihry**[2]

[1] Chemistry Department, Faculty of Science, Assiut University, Assiut, Egypt
[2] Chemistry Department, Faculty of Science, King Faisal University, P.O. Box 1759, Al-Hofof 31982, Saudi Arabia

Received March 21, 2003; accepted (revised) June 25, 2003
Published online February 5, 2004

Summary. A series of $AlPO_4$-V_2O_5 (*APV*) systems with various vanadia amounts 1–30 mol% were prepared by the impregnation method and calcinated at 400 and 600°C for 4 h. The catalysts were characterized by TG/DTG, DSC, IR spectroscopy, XRD, N_2 adsorption, and electrical conductivity measurements. The surface acidity and basicity of the catalysts were studied by the dehydration-dehydrogenation of isopropyl alcohol and the adsorption of pyridine. The catalytic gas phase esterification of acetic acid with ethyl alcohol was carried out at 210°C in a flow system at 1 atm using air as a carrier gas. The results showed that the catalysts calcinated at 400°C were active and selective towards the formation of ethyl acetate whereas the calcination of samples at 600°C led to a drastic reduction in both activity and selectivity. Good correlations were obtained between catalytic activities towards ester formation and acidity of the prepared catalysts.

Keywords. V_2O_5; $AlPO_4$; Structure; Texture; Catalysis; Esterification.

Introduction

Aluminum phosphate can be used as a catalyst and support. As a catalyst, $AlPO_4$ is known to be active in several chemical processes such as dehydration, isomerization, alkylation, condensation, and *Diels Alder* cycloaddition [1–6]. Moreover, $AlPO_4$ is also used as a support for polymerization, oxidation, hydrogenation, reductive cleavage, or hydration catalysts [1, 7–10]. Now, solid acid-base catalysis is one of the economically and ecologically important fields in catalysis. The acid-base properties of $AlPO_4$ play an important role in catalytic reactions. By modifying the acid-base properties of $AlPO_4$, the catalytic activity can be controlled. The modification with a metal oxide [1, 10–12], brings about changes in the physicochemical properties and catalytic activities of $AlPO_4$. Experimental studies of such

* Corresponding author. E-mail: a.a.said@acc.aun.edu.eg

systems indicated that coupled techniques can be used to characterize the different types of bulk and surface active phases resulting from the solid–solid interaction between V_2O_5 and $AlPO_4$. Moreover, various vanadium phosphates have been detected in the *VPO* catalysts, depending on the methods of preparation and conditioning of the conventional catalyst precursor. The current literature disagrees on the nature of active phase [13–17]. Thus, the activity of $AlPO_4$-vanadia catalysts were considerably affected by the chemical and physical nature of the phases formed during heat treatment of start materials. However, synthesis and physico-chemical properties of vanadium aluminum phosphate were documented in literature on the *VPO* pure compounds [18–21]. On the other hand there are few reports that studied the formation and physico-chemical properties of the *VPO* compounds resulting from the solid–solid interaction between vanadia and $AlPO_4$ support during heat treatments of the precursor. Therefore, the present work was devoted to study the physico-chemical properties of the phases which were formed by the solid–solid interaction between V_2O_5 and $AlPO_4$ during heat treatment and their activities towards the esterification of acetic acid with ethyl alcohol. For this purpose the resulting solids were characterized by DTG, DSC, X-ray diffraction, IR spectroscopy, surface area, porosity assessment, and surface acidity. We also studied the catalytic esterification of acetic acid with ethanol in order to understand its correlation with acidic properties.

Results and Discussion

Catalyst Characteristics

Thermal Analysis

DTG curves of pure *AP* and mixed with *AMV* are shown in Fig. 1. The DTG analysis of pure *AP* (curve a) shows that *AP* looses weight with heating over two stages. The first stage that becomes evident is at 100°C and corresponds to the desorption of physisorbed water. The second stage occurs at 140°C and is due to the loss of strongly adsorbed water. Curves b–e represent the DTG curves of *AP* which was supported with different ratios of *AMV*. The analysis of the data of these curves indicate some trends and the following conclusions may be drawn: (i) The weight loss on heating up to 200°C exhibits two peaks similar to that of pure *AP*. (ii) On addition of *AMV*, new peaks start to appear reaching maxima at the addition of 30 mol%. The maxima of these peaks at 190, 200, 307, and 330°C correspond to the decomposition of *AMV via* intermediates into V_2O_5 [22]. On the other hand, it is important to mention here that no weight loss was observed on increasing the heating temperature above 330°C up to 600°C. Figure 2 represents the DSC results of pure *AP* and *AP* mixed with *AMV*. Curve a shows that *AP* exhibits one broad endothermic peak at about 130°C. The endothermic behavior below 200°C illustrates the well known weight loss due to the removal of crystalline water. Curves b–e for the supported samples show new endothermic peaks between 200° and 500°C. These new peaks may be attributed to the decomposition of *AMV* into V_2O_5 below 350°C, the interaction between V_2O_5 and $AlPO_4$ to produce a new phase, and/or phase transformation above 350°C.

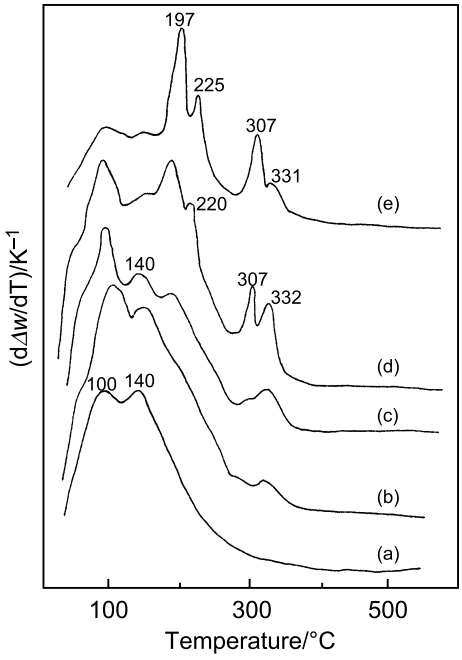

Fig. 1. DTG curves of pure *AP* (a) and *AMV* supported on *AP*: 10% (b), 15% (c), 20% (d), and 30% (e)

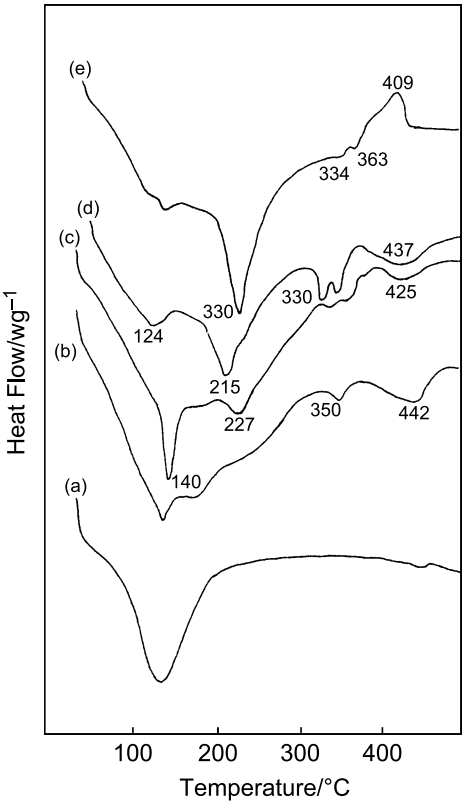

Fig. 2. DSC curves of pure *AP* (a) and *AMV* supported on *AP*: 10% (b), 15% (c), 20% (d), and 30% (e)

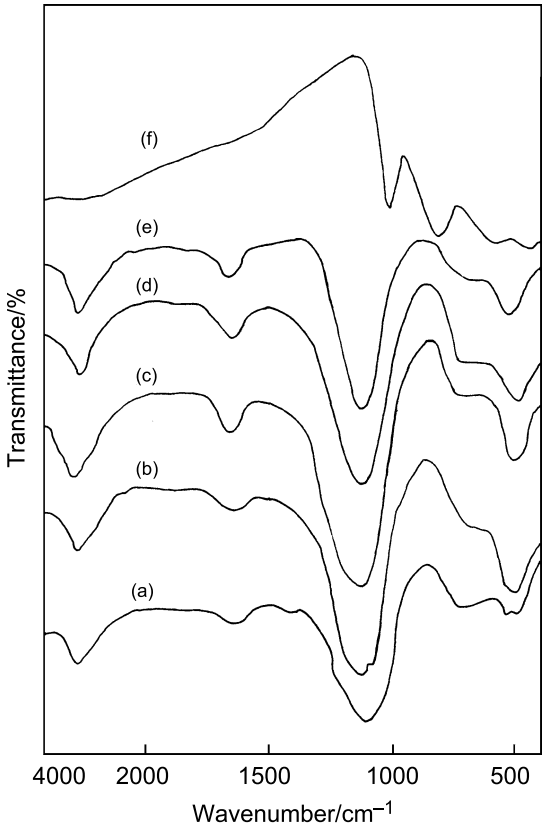

Fig. 3. IR spectra of pure *AP* (a) and *AMV* supported on *AP*: 5% (b), 10% (c), 20% (d), 30% (e), and pure *AMV* (f) of the samples calcinated at 400°C

IR Spectra

IR spectra of pure *AP* and *AP* mixed with AMV calcinated at 400 and 600°C are shown in Figs. 3 and 4. The samples calcinated at 400°C, Fig. 3, show that, the spectrum of pure *AP* exhibits three absorption bands. The first one, assigned at $\bar{\nu} = 3450\,\mathrm{cm}^{-1}$, is characteristic of an unbonded surface P–OH group, the second band, which appeared at $\bar{\nu} = 1628\,\mathrm{cm}^{-1}$, is due to the deformation vibration of water, and the third band in the region between $\bar{\nu} = 1200$ and $1000\,\mathrm{cm}^{-1}$, is probably due to the different internal stretching modes of the PO_4 tetrahedra, AlO_4 tetrahedra, and AlO_4 (H_2O) octahedra [23, 24]. It is worth noting that there are no bands observed corresponding to pure V_2O_5 or new phases resulting from the interaction between V_2O_5 and $AlPO_4$. On the other hand the spectra of the supported samples calcinated at 600°C, Fig. 4, show that the bands due to the water molecules located in the interlayer space have disappeared. Moreover, new bands appeared at $\bar{\nu} = 960$, 710, and $620\,\mathrm{cm}^{-1}$ for the samples of *AP* mixed with 5, 10, 20, and 30 mol% V_2O_5. These new bands may correspond to the formation of a new phase.

X-Ray Diffraction

X-Ray diffraction patterns of *AMV* supported on *AP* calcinated at 400 and 600°C were carried out. The diffractograms of the samples calcinated at 400°C (not

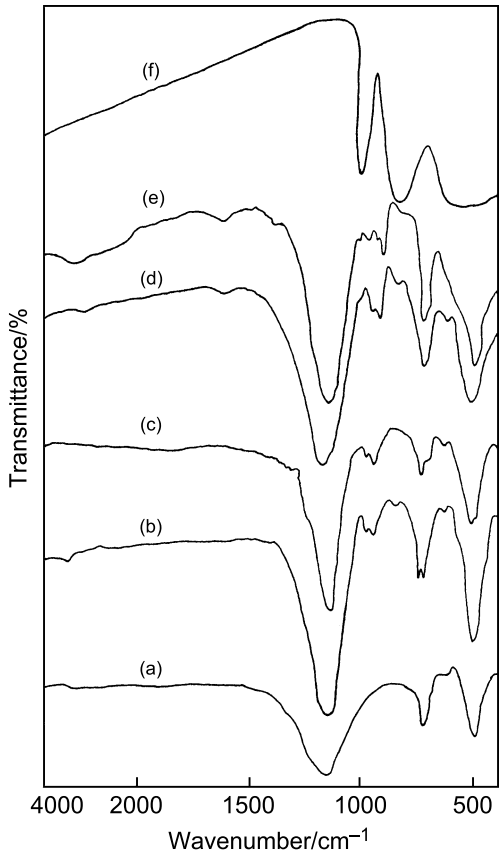

Fig. 4. IR spectra of pure *AP* (a) and *AMV* supported on *AP*: 5% (b), 10% (c), 20% (d), 30% (e), and pure *AMV* (f) of the samples calcinated at 600°C

shown) show that pure *AP* exhibits an amorphous structure. Even after addition of 5, 10, and 20 mol% V_2O_5, little crystallinity is observed and *AP* remains amorphous. Moreover, the line which is located at $2\theta = 26.58°$ may correspond to the formation of a β-$VOPO_4$ phase [25]. The little crystallinity of this new phase may explain that absorption bands corresponding to this new phase were undetectable on the IR spectra of the samples calcinated at 400°C. Furthermore, on increasing the calcination temperature to 600°C, the tested samples exhibit well crystalline structures, as shown in Fig. 5. It showed that a β-$VOPO_4$ phase had developed and gave a predominant diffraction line located at $2\theta = 26.39°$ for the samples containing $V_2O_5/AlPO_4$ at ratios $<$20 mol%. In addition, the predominant new line located at $2\theta = 21.68°$ of 20 or 30 mol% V_2O_5 in *AP* corresponds to the formation of a new phase [25], β''-$(VO)_2P_2O_7$. It is worth mentioning that the calcination of prepared catalysts was carried out under a static air atmosphere, thus, the formation of this new phase may have occurred according to the following solid state reaction.

$$2VOPO_4 \rightarrow (VO)_2P_2O_7 + \frac{1}{2}O_2$$

Moreover, in addition to this new phase, the diffraction lines located at $2\theta = 29.77$ and 35.96° correspond to the existence [22, 26] of $AlVO_4$ spinel and Al_2O_3, respectively.

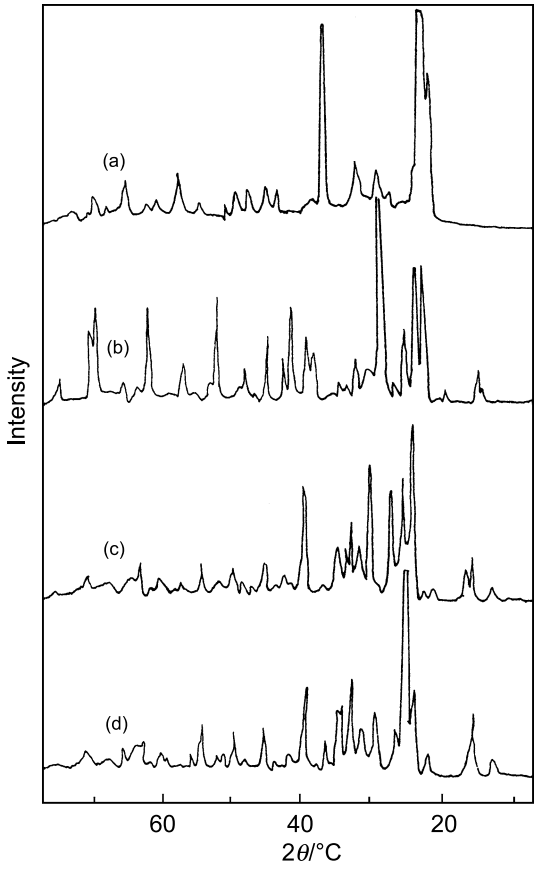

Fig. 5. X-Ray diffraction patterns of pure *AP* (a) and *AMV* supported on *AP*: 10% (b), 20% (c), and 30% (d) of the samples calcinated at 600°C

Surface Area and Porosity

The adsorption–desorption isotherms of nitrogen were measured on pure *AP* and *AP* mixed with different ratios of *AMV* calcinated at 400 and 600°C. The specific surface areas, S_{BET}, of the samples calcinated at 400°C, and the values of the *BET* constant, C_{BET}, are shown in Table 1. The results indicate that *AP* suffered a continuous decrease in its S_{BET} value by increasing the loading of V_2O_5. However, the values of C_{BET} show that the samples 1, 5, and 30 are little greater than 200. This may taken as an indication that these catalysts are accompanied by micropores. On the other hand for the rest of samples, the C_{BET} value is less than 200. This may be taken as an indication that basically monolayer–multilayer formation is operative and it is not accompanied by any meaningful micropore filling.

Table 1. S_{BET} and C_{BET} values of $AlPO_4$-V_2O_5 system calcinated at 400°C

Catalyst	*AP*	1	5	10	15	20	30	V_2O_5
$S_{BET}/m^2\,g^{-1}$	62.9	61.8	53.0	48.4	48.8	40.0	38.6	2.0
C_{BET}	127.8	250.0	216.7	118.5	105.0	90.8	203.0	63.0

Table 2. S_{BET} and C_{BET} values of $AlPO_4$-V_2O_5 system calcinated at 600°C

Catalyst	*AP*	1	5	10	15	20	30	V_2O_5
$S_{BET}/m^2\,g^{-1}$	17.7	8.2	7.0	7.4	8.2	9.9	11.0	6.1
C_{BET}	17.6	14.7	14.0	13.2	18.0	19.8	28.9	18.5

On the other hand, the surface area and C_{BET} values of the samples calcinated at 600°C are given in Table 2.

It shows a drastic reduction of the S_{BET} and C_{BET} values. The pore volume analysis indicates that the materials contain wide mesopores. These pores may be created by the sintering process which is responsible for such decrease in the S_{BET} values.

Electrical Conductivity

The electrical conductivity measurements with and without reactant vapors have been studied in the range 150–300°C on the catalysts, calcinated at 400°C. The experimental conditions used are similar to those used in catalytic activity runs. The results indicated that the electrical conductivity value, increases on increasing the reaction temperature. Plots of $\log k$ against $1/T$ of pure *AP* and *AP* mixed with V_2O_5 can be fitted to an *Arrhenius* relationship [27],

$$k = k_o \exp^{-\Delta Ea/RT}$$

where k is the electrical conductivity, k_o is the pre-exponential factor and ΔE_a is the activation energy for migration of charge carriers. Values of ΔE_a obtained by least squares fitting of the data are shown in Fig. 6. It shows the variation of ΔE_a with the % loading of V_2O_5. Curve a shows that without the reaction mixture (air only), addition of a low amount of V_2O_5 led to an observable decrease in the value

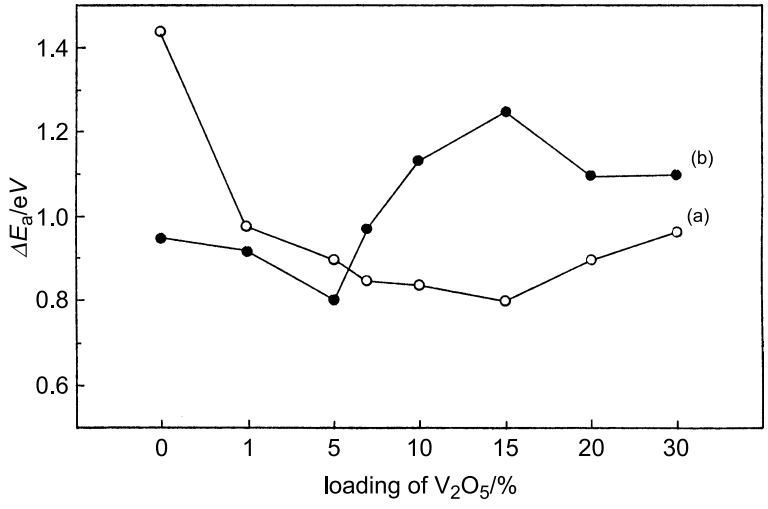

Fig. 6. Variation of the activation energy (ΔE_a) with the loading of V_2O_5 of the samples calcinated at 400°C, (a) air, (b) air + reactants

of ΔE_a of pure *AP* followed by a little decrease observed on increasing to a % content of V_2O_5. However, according to XRD results, it can be suggested that the formation of β-$VOPO_4$ which contains V ions in the V^{5+} valence state should decrease the V^{4+}/V^{5+} ratio and consequently should decrease the electron jumping on the catalyst surface. On the other hand curve b shows that on admission of the reaction mixture, (ethanol + acetic acid + air), ΔE_a of pure *AP* decreases from 1.48 to 0.96 eV. Moreover, a remarkable increase in ΔE_a value is observed on further increase in V_2O_5 ratio reaching a maximum on addition of 15 mol%, then a decrease up to the addition of 30 mol% is observed. However, the comparison between ΔE_a in presence and absence of the reactant mixtures provides a clear and direct evidence for a redox mechanism with consumption of surface lattice oxygen. Such a redox mechanism requires the presence of V^{5+} ions in equilibrium with V^{4+} ions. However, the formation of β-$VOPO_4$ spinel is responsible for the presence of V^{5+} ions as an acceptor site (acid site) for the electron injected by the alcohol adsorbed on the catalyst surface. Moreover, the concept of acidic and basic sites of the catalyst surfaces has been reviewed [28, 29] in relation to a perturbational molecular orbital theory of acid base interactions. It has been shown [28] that spatial extent of electronic states at the surface, that is, whether they are delocalized or localized, is a determining factor in adsorption and chemical reaction selectivity. On metal oxides, from the structure and composition stand points, the spatial extent of electronic states may be controlled by the degree of departure from stoichiometry [30] as influenced by pretreatment conditions and/or foreign ion additives. Thus, the width of the energy gap is also important in controlling the redox mechanism, the number of molecules which can be chemisorbed in the course of a catalytic reaction, and the nature of the chemical bond between the molecule and the surface. Accordingly, the modification observed in the *Fermi* potential Fig. 6 should play a role in the activity and selectivity of the prepared catalysts.

Surface Acidity

The catalytic dehydration-dehydrogenation of *IPA* over V_2O_5 supported on $AlPO_4$ is represented in Fig. 7. The results indicate that the reaction products were mostly propene and scarcely acetone. However, it has been suggested that the *IPA* dehydration has been used by several authors [28, 31] as a test reaction for determining the acidity of different catalysts and it proceeds quickly on weak acid sites [26]. Isopropanol decomposition can form either propene and water (dehydration) or acetone and hydrogen (dehydrogenation). The different characteristics of the species present in the solids are modified in their behaviour as catalysts in the *IPA* dehydration reaction, which is used as a comparative measure of the catalyst acidity. Thus, it can be observed from Fig. 7 that the % yield of propene on pure *AP* indicates that the reaction of *IPA* is reflecting the fact that only little weak acid sites exist on the *AP* surface. Eventually, the introduction of a low amount of vanadia, 1 mol%, into *AP* practically does not alter its activity, however, larger amounts (3–30 mol%) lead to an observable increase in its activity and selectivity of propene formation, the more the greater the V_2O_5 loading. However, the acid centers, present at the *APV* surface, have been identified as hydroxyl groups bonded either to

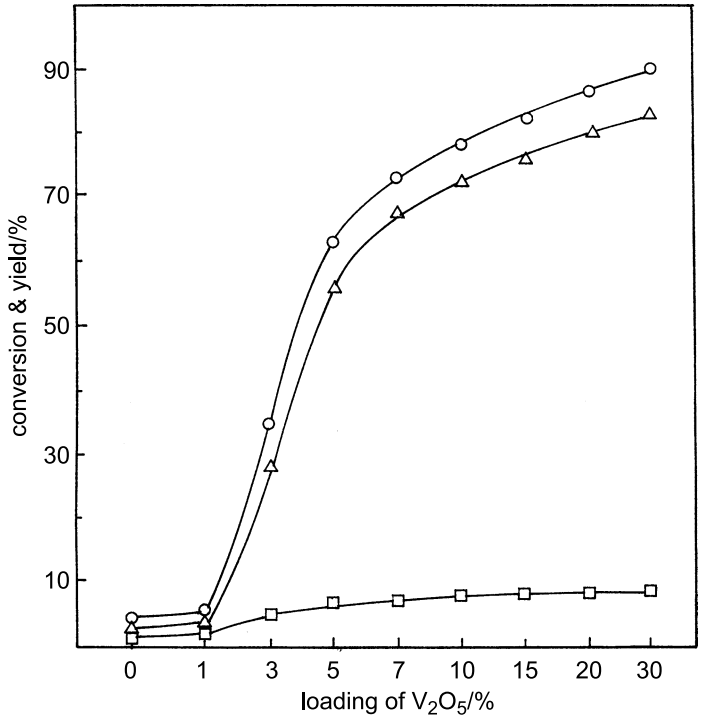

Fig. 7. Variation of *IPA* conversion (o) and yields of propene (Δ) and acetone (□) with the loading of V_2O_5 supported on *AP* of the samples calcinated at 400°C

Al, P, or V atoms. These hydroxyl groups are most probably responsible for *Brönsted* acidity [3, 16]. The *Lewis* acid sites on *APV* powders are most probably linked to the presence of metal cations, V^{5+}, which are electron acceptors. The second site is a basic site due to the presence of oxygen. Moreover, the presence of V–O–V bonds should increase the basicity of the supported catalysts. As regards the $AlPO_4$ support, the surface acidity is low although *Brönsted* acid sites are exhibited. However, the acid properties of $AlPO_4$ can be modified by introducing elements different from Al and P in the framework at different loading. Thus, it is evident from Fig. 7 that the incorporation of V_2O_5 to $AlPO_4$ results in a remarkable increase in the number of both *Brönsted* and *Lewis* acid sites.

It is known that the chemisorption of pyridine (*PY*) was used as a base probe determine the acidity of the catalysts [29, 32]. The poisoning of the active sites of the *APV*20 catalyst in the *IPA* conversion was performed through the saturation of the acid sites with *PY* according to the following procedure. After measuring the conversion activity of the *APV*20 catalyst at 210°C the catalyst was injected with different volumes of *PY* in the stream of the reactants using N_2 as a carrier gas. The obtained results represented in Fig. 8 indicate that the *PY* strongly suppressed the activity for the *IPA* dehydration. So, the chemisorbed *PY* decreases the yield of the dehydration process from 82 to 20%. The dehydrogenation activity practically does not change by base poisoning. A drop in the dehydration activity is accompanied by a change in product selectivity towards the propene yield, getting greater as the poisoning effect increases (Fig. 7). The above results demonstrate that in the

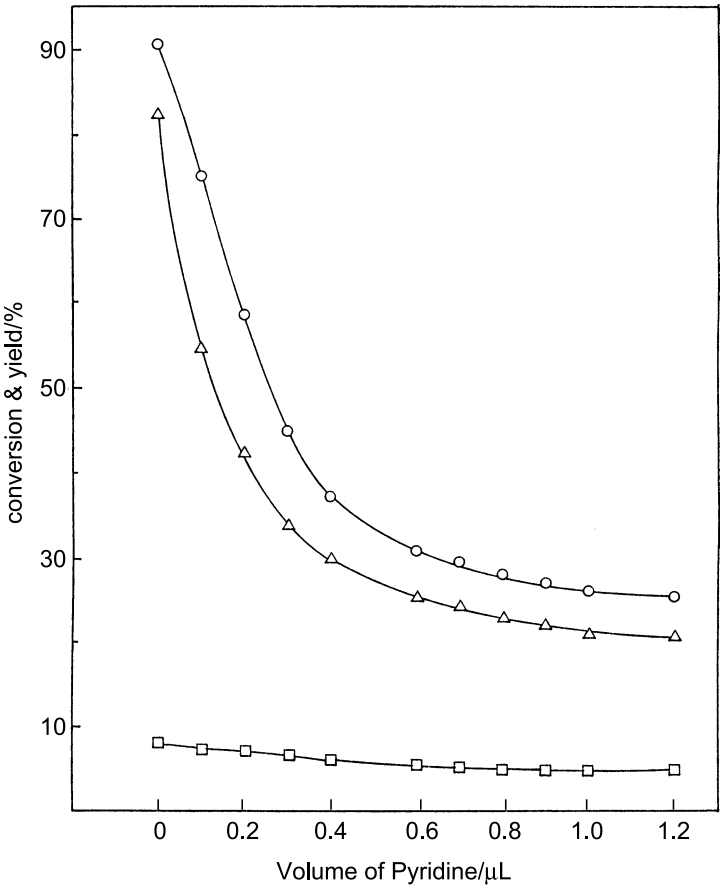

Fig. 8. Variation of *IPA* conversion (o) and yields of propene (Δ) and acetone (□) with volume of pyridine for the *APV*20 catalyst

investigated catalysts weak, intermediate, and strong acidic sites are operative. The admission of *PY* poisons only the intermediate and strong ones.

Catalytic Activity

The catalytic esterification of acetic acid with ethanol over the catalysts calcinated at 400 and 600°C for 4 h, was carried out at 210°C. The reaction conditions were: 0.5 g of catalyst, 2.1% acetic acid, and 1.6% ethanol reactants were fed into the reactor after air had been bubbled through thermostated acetic acid and ethanol at a total flow rate of 130 $cm^3\ min^{-1}$. The analysis of the gas mixture after the reaction revealed that ethyl acetate and acetaldehyde were the only products. The experimental results of the catalysts calcinated at 400°C are presented in Fig. 9. It shows that pure *AP* support is active and selective towards the formation of ethyl acetate. Moreover, the introduction of vanadia (1–5 mol%) into $AlPO_4$ steadily increases its activity towards the ester formation. Larger amounts (7–30 mol%) lead to an observable increase in both activity and yield of ester. This effect increases as V_2O_5 loading increases. The *IPA* conversion and the propene production depend in a similar way on the vanadia loading and it is similar to that acidic characteristic

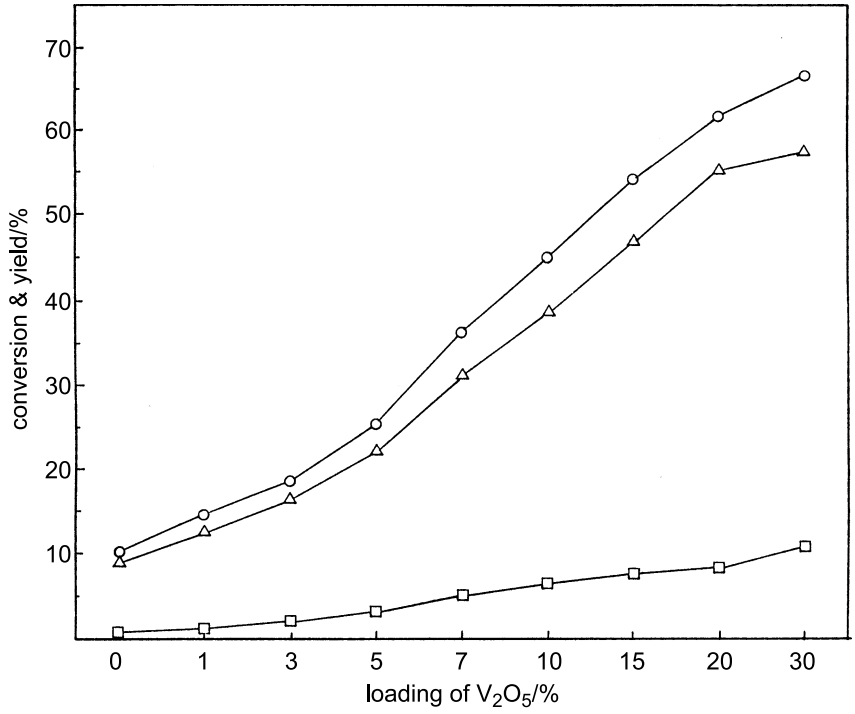

Fig. 9. Variation of ethanol conversion (o) and yields of ethyl acetate (Δ) and acetaldehyde (□) with the loading of V_2O_5 supported on *AP* of the samples calcinated at 400°C

behavior, see Fig. 7. In addition, the correlation between yield of ethyl acetate and loading of V_2O_5 shows a straight line, Fig. 10. There seems to be is a linear relationship between the catalytic activity to ester formation and the number of created active acidic sites due to the addition of vanadia into *AP*.

It is reasonable to mention here that although *AP* is active and selective towards ethyl acetate formation, it exhibits low activity to the formation of propene via *IPA* decomposition. This means that the *AP* surface possesses intermediate strength or strong acid sites which are comfortable sites for the esterification reaction. Thus, the catalytic activity of *AP* may be affected by two factors, the chemical nature of the surface (number and strength of acid sites) and the texture of the solid. Consequently, it appears that the addition of V_2O_5 (acid catalyst) may activate the sites present on the $AlPO_4$ surface and/or creates new acid sites. The new acid sites can be formed *via* the creation of V–OH *Brönsted* acid sites close to active centers [33] and the formation of new phases, β-$VOPO_4$ and β''-$(VO)_2P_2O_7$. Moreover, during the reaction, β-$VOPO_4$ is slowly converted to vanadyl pyrophosphate in a reaction mixture in which vanadium ions are in the V^{4+} state. In addition, the formation of the above new phases accompanies the formation of Al_2O_3, as indicated by XRD. The Al_2O_3 may form some kind of solid solution and/or a new phase [34], $AlVO_4$, with the excess V_2O_5 in the solid matrix. The creation of V^{4+} by the $AlVO_4$ and β''-$(VO)_2P_2O_7$ spinels should increase the ratio of V^{4+}/V^{5+}. Moreover, from the electrical conductivity results, the observed higher degree of conversion as well as the yield of ester for the samples containing V_2O_5 (>5 mol%). This may either result from the optimum ratio of V^{4+}/V^{5+} cations or could also be related to the

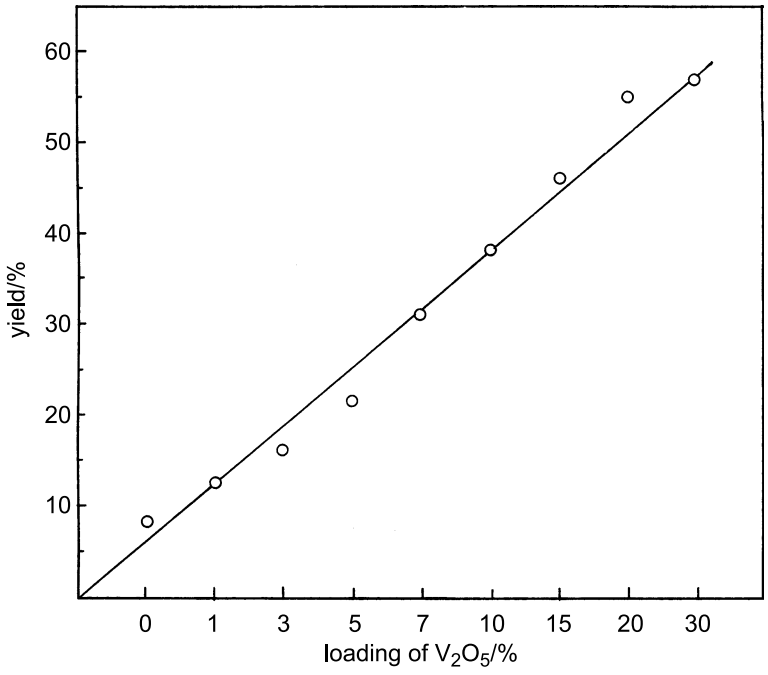

Fig. 10. Variation of yield of ethyl acetate with loading of V_2O_5 supported on *AP* of the samples calcinated at 400°C

value of *Fermi* potential. Thus, the increase in the energy gap of $AlPO_4$ by the addition of V_2O_5 during the reaction course may enhance the electron exchange between the reactants and the catalyst surface.

In addition, the porosity framework of $AlPO_4$ can be modified *via* substituting aluminum or phosphorus by metal atoms in different valence states [35]. Consequently, it is interesting to note that the samples which have the smallest pore aperture are more active towards esterification. This observation suggests that the reaction under study is not limited by internal diffusion in the *APV* samples.

Finally, it is quite unexpected that the esterification selectivity of samples calcinated at 600°C (results not shown) is decreases drastically, even though the samples contain β-$(VO)_2P_2O_7$ as the predominant crystalline phase. This behavior may be attributed to the drastic decrease in the surface area. It is also possible that the formation of β''-$(VO)_2P_2O_7$ is responsible for a reduction of the V^{4+}/V^{5+} ratio. Moreover, the removal of OH groups (*i.e. Brönsted* acid sites), caused by the calcination of the catalysts at 600°C, Fig. 4, also led to such a decrease.

Conclusions

The modification of $AlPO_4$ with V_2O_5 leads to an improvement in the textural properties and the catalytic activity. The *AP* treated with V_2O_5 resulted in an enhancement of the dehydration reaction towards the ethyl acetate formation *via* the intermediate or strong acid sites. Moreover, the increase of the energy gap of $AlPO_4$ by the addition of V_2O_5 (>5 mol%) during the reaction may enhance the

electron exchange between the reactants and the acid-base sites on the catalyst surfaces.

Experimental

Materials

The starting materials $AlPO_4$, *AP*, (Merck) and NH_4VO_3, *AMV*, (BDH) were used for the preparation of the catalysts. The mixed samples were prepared by impregnation of $AlPO_4$ with different proportions of *AMV* dissolved in doubly-distilled water. Yellow mixtures were formed which denoted the formation of a new phase [36]. The samples produced were dried in an oven at 100°C for 24 h before being calcinated at 400 and 600°C for 4 h in a static air atmosphere. The content of V_2O_5 added, was varied between 1 to 30 mol%.

Apparatus and Techniques

Thermal Analysis

A thermal analyzer 2000 TA instrument (USA) controlling a 2050 thermogravimetric (DTG) analyzer and a 2010 differential scanning calorimeter (DSC) was used. DTG curves were recorded upon heating up to 600°C at 10 K min^{-1} and a 30 cm^3 min^{-1} flow of nitrogen gas. For DSC measurements, a sample was heated up to 500°C at 10 K min^{-1} and a flow of 30 cm^3 min^{-1} of nitrogen gas.

IR Spectroscopy

Spectra of the samples calcinated at 400 and 600°C for 4 h were recorded in the $\bar{\nu} = 4000$–$400\ cm^{-1}$ region with a Shimadzu spectrophotometer (model 740) using the KBr disc technique.

X-Ray Diffraction

XRD of the test samples was performed with a Philips diffractometer (Model PW 2103) equipped with Ni-filtered CuK_α radiation ($\lambda = 1.5418$ Å, 23 kV, and 20 mA).

Nitrogen Gas Adsorption

Nitrogen gas adsorption–desorption isotherms were measured at –196°C using a model ASAP 2010 instrument (Micromeritics Instrument Corporation, USA). Test samples were thoroughly outgassed for 2 h at 200°C. The specific surface area, S_{BET}, was calculated applying the *BET* equation [R_1].

Electrical Conductivity

The electrical conductivity measurements were carried out using a conductivity cell described previously [37].

Catalytic Activity Measurements

The activity of catalysts towards the esterification of acetic acid with ethanol in the gas phase was determined in a conventional fixed-bed flow type reactor. The gases after reaction were chromatographically analyzed by a FID on a Unicam proGC using 2 m *DNP* and 10% *PEG* 400 glass columns for the analysis of the reaction products of ethanol, acetic acid, and isopropanol on the tested catalysts.

References

[1] Bautista FM, Campelo JM, Garcia A, Luna D, Marinas JM, Romero AA (1993) Appl Catal **A96**: 175
[2] Cativiela C, Fraile JM, Garcia JI, Mayoral JA, Campelo JM, Luna D, Marinas JM (1993) Tetrahedron Asymm **4**: 2507
[3] Campelo JM, Garcia A, Herencia JF, Luna D, Marinas JM, Romero AA (1995) J Catal **151**: 307
[4] Bautista FM, Delmon D (1995) Appl Catal **A130**: 47
[5] Afxanidis J, Bouchry N, Aune JP (1995) J Mol Catal **A120**: 49
[6] Bautista FM, Campelo JM, Garcia A, Leon J, Luna D, Marinas JM (1995) J Chem Soc Perkin Trans **2**: 815
[7] Lindblad T, Rebenstof B, Yan ZG, Andersson SLT (1994) Appl Catal **A112**: 87
[8] Lakshim LJ, Rao PK (1993) Catal Lett **21**: 345
[9] Lakshmi LJ, Srinivas ST, Rao PK, Nosov AV, Lapina OB, Mastikhin VM (1995) Solid State Nucl Magn Reson **4**: 59
[10] Campelo JM, Chakrarty R, Marinas JM (1996) Syn Commun **26**: 415, 26 (1996) 1639
[11] Blanco A, Campelo JM, Garcia A, Luna D, Marinas JM, Ramero AA (1992) J Catal **137**: 51
[12] Bautista FM, Campelo JM, Garcia A, Luna D, Marinas JM, Ramero AA, Navio JA, Mucias M (1994) J Catal **145**: 107
[13] Guliants VV, Benziger JB, Sundaresan S, Yao N, Wachs IE (1995) Catal Lett **32**: 279
[14] Sananes MT, Hutchings GT, Volta JC (1995) J Catal **154**: 253
[15] Blasca T, Concepcion P, Grotz P, Lopez JM, Mortinez-Arias A (2000) J Mol Catal A, Chem **162**: 267
[16] Said AA, Khalil KMS (2000) J Chem Technol Biotechnol **75**: 103
[17] Kamia Y, Nishikawa E, Okuhara T, Hattori T (2002) App Catal **A206**: 103
[18] Zahedi-Niaki MH, Javaidzaidi SM, Kalia Guine S (2000) App Catal **A196**: 9
[19] Hannepon MJ, Elemans-Mehring AM, Von Hooff JHC (1997) Appl Catal **A152**: 183, 152 (1997) 203
[20] Concepcion P, Lopez-Nieto JM, Mifsud A, Perez-Pariente J (1997) Appl Catal **A151**: 373
[21] Ishimura T, Sugiyama S, Hyashi H (2000) J Mol Catal A, Chem **158**: 2559
[22] Said AA (1992) J Mat Sci **27**: 5869
[23] Davis ME, Monte C, Hathaway PE, Arhancet JP, Hasha DL, Garces JM (1989) J Am Chem Soc **111**: 3919
[24] Pluth JJ, Smith JV (1986) Acta Crystallog Seet C, Cryst Struct Commun **9**: 1118
[25] Ben-Abdelouhab F, Olier R, Guilhaume N, Lefebvre F, Volta JC (1992) J Catal **134**: 151
[26] Yamaguchi O (1987) J Am Ceram Soc **70**: 198
[27] Morrison SR (1978) In: Chemical Physics of Surfaces. Plenum, New York, 70
[28] Stair PC (1982) J Am Chem Soc **104**: 4044
[29] Sorensen OT (1981) ''Non Stoichiometric Oxides'' In: Sorensen TO (ed). Academic Press, New York London, p 2
[30] Flanigen EM, Patton RL, Wilson ST (1988) Stud Surf Sci Catal **37**: 13
[31] Sohn JR, Jang HJ (1991) J Mol Catal A, Chem **64**: 349
[32] Coroma A, Fornes V, Colodziejski W, Martinez-Triguero LJ (1994) J Catal **145**: 27
[33] Martra G, Arena F, Colluccia S, Frusteri F, Parmaliana A (2000) Catal Today **63**: 197
[34] Abd El-Wahab MMM, Said AA (1994) Collect Czech Chem Commun **59**: 1983
[35] Melanova K, Benes L, Vicek M, Patrono P, Massucci MA, alli P (1999) Metter Res Bull **34**: 895
[36] R'Kha C, Vanadeborre MT, Livage J (1986) J Solid State Chem **63**: 202
[37] Said AA, Hassan EA, Abd El-Salaam KM (1983) Surf Technol **20**: 123